2005 American Control Conference
June 8-10, 2005. Portland, OR, USA

Optimization-Based Calibration of a Triaxial Accelerometer-Magnetometer

Erin L. Renk, Walter Collins, Matthew Rizzo, Fuju Lee, and Dennis S. Bernstein

I. Introduction

In this paper, we use a robotic arm to calibrate a triaxial accelerometer and magnetometer. In particular, we estimate the sensitivity and bias of each of the three accelerometers and magnetometers that comprise the triaxial sensor. We also determine the angles between each pair of accelerometers and each pair of magnetometers.

To perform this calibration, the sensor is mounted to the end effector of a robotic arm. The robot has six joints, or links. Accelerometer measurements are recorded as the robot moves three of the six joints, performing rotational movements in roll, pitch, and yaw, which correspond to rotations about the x-axis, y-axis, and z-axis of a cartesian frame, respectively. A related method for calibrating a sensor was used in [1], where a calibration platform for an inertial measurement unit with 4 GPS antennas was designed using a carpal wrist and turntable.

The triaxial accelerometer and magnetometer considered in this paper are encompassed in a 3DM Solid State 3-axis Pitch, Roll, and Yaw Sensor supplied by Microstrain, Inc. Taps were added to the sensor by the vendor, allowing us to obtain analog voltage readings directly rather than post-processed digital readings. The taps are connected to a Q8 High-Performance H.I.L. Control Board manufactured by Quanser, Inc., which implements analog-to-digital conversion for data acquisition. The board has 14-bit resolution and an input range of $\pm$ 10 V. The robotic arm is a six-degree-of-freedom A465 Robot Arm manufactured by CRS Robotics Corporation.

II. Kinematic Model

We first consider the problem of calibrating the accelerometers, beginning with the derivation of a kinematic model. Let the subscript rb denote the robot base frame, let the subscript ee denote the end effector frame, and let

$$\begin{bmatrix} \hat{\imath}_{\mathrm{ee}} \\ \hat{\jmath}_{\mathrm{ee}} \\ \hat{k}_{\mathrm{ee}} \end{bmatrix}, \begin{bmatrix} \hat{\imath}_{\mathrm{rb}} \\ \hat{\jmath}_{\mathrm{rb}} \\ \hat{k}_{\mathrm{rb}} \end{bmatrix} \tag{1}$$

denote mutually orthogonal unit coordinate vectors fixed to the end effector frame and fixed to the robot base frame, respectively. For $i = 1, \ldots, 6$, let

$$\begin{bmatrix} \hat{\imath}_i \\ \hat{\jmath}_i \\ \hat{k}_i \end{bmatrix} \tag{2}$$

denote mutually orthogonal coordinate vectors fixed to the i^{th} link frame of the robot. Furthermore, assume that the base of the robot, which is not necessarily level, is located at the origin of an inertial frame. All motion is sufficiently slow that the only acceleration that each accelerometer senses is due to gravity. Let $\vec{g}$ denote the gravitational acceleration vector, which, in the robot base frame, is resolved as

$$\vec{g}|_{\mathrm{rb}} = \begin{bmatrix} g_{\mathrm{x}} \\ g_{\mathrm{y}} \\ g_{\mathrm{z}} \end{bmatrix}. \tag{3}$$

The gravity vector is not a parameter of interest in our accelerometer calibration. However, its direction does affect the estimates of other parameters that are of concern. To illustrate, suppose that the gravity vector points in the $-\hat{k}_{\mathrm{rb}}$ direction and that an accelerometer's axis points in the $+\hat{k}_{\mathrm{rb}}$ direction so that the accelerometer measures 1 g. Rotate the orientation vector of the accelerometer 180 deg about the $\hat{k}_{\mathrm{rb}}$-axis, followed by a 90 degree rotation about the $\hat{\imath}_{\mathrm{rb}}$-axis. The accelerometer now measures 0 g. Now, assume that gravity points in the $-\hat{\imath}_{\mathrm{rb}}$ direction and the accelerometer's axis points in the $+\hat{\imath}_{\mathrm{rb}}$ direction so that the accelerometer again measures 1 g. After performing the same sequence of rotations, the accelerometer reads -1 g. Since this reading is inconsistent with the previous reading after the 2 rotations, the direction in which gravity points does affect the data readings and must be taken into account in formulating the system model. Similar comments apply to the magnetometer and the Earth's magnetic field. Since we did not attempt to precisely level the robot base, the direction of gravity is unknown, and thus we estimate the direction of gravity as part of the calibration.

Each accelerometer measures a scalar component of the acceleration vector due to gravity in the direction of its axis (referred to as an orientation vector) resolved in the end effector frame. We resolve the orientation vector of each accelerometer in the robot base frame by transforming each vector from the end effector frame.

Let the subscript $k = 1, 2, 3$ denote an accelerometer. Rotating the unit vector $\hat{\imath}_{\mathrm{ee}}$ through an angle β about the $\hat{\jmath}_{\mathrm{ee}}$-axis and then through an angle γ about the $\hat{k}_{\mathrm{ee}}$-axis yields the unit orientation vector $\hat{P}_k$ of the k^{th} accelerometer in the end effector frame. For the k^{th} accelerometer, the

This work was supported by the Rackham Graduate School, University of Michigan, under a Rackham Engineering Award Fellowship and by the National Aeronautics and Space Administration under a Graduate Student Research Fellowship.

The Authors are with the Department of Aerospace Engineering, University of Michigan, Ann Arbor, MI 48109-2140, USA dsbaero@umich.edu

TABLE I

DENAVIT-HARTENBERG TABLE FOR THE SIX-DEGREE-OF-FREEDOM ROBOTIC ARM.

i	α_i	θ_i
1	$\frac{\pi}{2}$	θ_1
2	0	$\frac{\pi}{2}$
3	0	$-\pi$
4	$\frac{\pi}{2}$	0
5	$\frac{-\pi}{2}$	θ_5
6	0	θ_6

transformation (or rotation) matrix that describes a rotation about the $\hat{\jmath}_{\rm ee}$-axis by an angle β_k is given by

$$R_{\hat{\jmath}}(\beta_k) = \begin{bmatrix} \cos(\beta_k) & 0 & \sin(\beta_k) \\ 0 & 1 & 0 \\ -\sin(\beta_k) & 0 & \cos(\beta_k) \end{bmatrix}, \quad (4)$$

and the transformation matrix for a rotation about the $\hat{k}_{\rm ee}$-axis by an angle γ_k is given by

$$R_{\hat{k}}(\gamma_k) = \begin{bmatrix} \cos(\gamma_k) & -\sin(\gamma_k) & 0 \\ \sin(\gamma_k) & \cos(\gamma_k) & 0 \\ 0 & 0 & 1 \end{bmatrix}. \quad (5)$$

Therefore, the unit orientation vector $\hat{P}_k$ resolved in the end effector frame is given by

$$\hat{P}_k|_{\rm ee} = R_{\hat{k}}(\gamma_k) R_{\hat{\jmath}}(\beta_k) \hat{\imath}|_{\rm ee}. \quad (6)$$

To resolve $\hat{P}_k$ in the robot base frame, we require the transformation matrix from the end effector frame to the robot base frame. The Denavit-Hartenberg table for the robot, given by Table I, can be used to formulate this transformation matrix [2]. Table I specifies the rotations from the end effector frame to the robot base frame, thereby determining the rotation matrix for each link of the robot arm.

In Table I, $1 \leq i \leq 6$ denotes a robot link, $i = 0$ corresponds to the robot base, α_i is the angle between the $\hat{k}_i$-axis of the i^{th} link and the $\hat{k}_{i-1}$-axis of the $i-1^{th}$ link for a rotation about the $\hat{\imath}_i$-axis, and θ_i is the angle between the $\hat{\imath}_{i-1}$-axis and the $\hat{\imath}_i$-axis for a rotation about the $\hat{k}_{i-1}$-axis. Here, the right-hand rule determines positive rotations. As a result of its definition and the way in which the robot arm is rotated, α_i is constant for each link. Links 2, 3, and 4 of the robot are locked during the experiment, and, thus, θ_2, θ_3, and θ_4 are constants. The angles θ_1, θ_5, and θ_6 are varied, and voltage readings are recorded. The general form of the rotation matrix from the i^{th} link frame to the $i-1^{th}$ link frame is given by

$$R_{i(\theta_i,\alpha_i)} = \begin{bmatrix} \cos(\theta_i) & -\sin(\theta_i)\cos(\alpha_i) & \sin(\theta_i)\sin(\alpha_i) \\ \sin(\theta_i) & \cos(\theta_i)\cos(\alpha_i) & -\cos(\theta_i)\sin(\alpha_i) \\ 0 & \sin(\alpha_i) & \cos(\alpha_i) \end{bmatrix}. \quad (7)$$

Therefore, the orientation vector $\hat{P}_k$ resolved in the end effector frame can be transformed into the robot base frame as

$$\hat{P}_k|_{\rm rb} = R_1 R_2 R_3 R_4 R_5 R_6 \hat{P}_k|_{\rm ee}. \quad (8)$$

For the k^{th} accelerometer, let S_k and δ_k denote the sensitivity and offset, respectively, and let a_k denote the component of acceleration in the direction of the k^{th} accelerometer's axis. Then, the voltage reading V_k for the k^{th} accelerometer is modeled as

$$V_k = S_k a_k + \delta_k. \quad (9)$$

Since, by assumption, the only acceleration felt by the accelerometers is due to gravity, the component of gravity measured by the k^{th} accelerometer is

$$a_k = |\vec{g}||\hat{P}_k| \cos\phi_k = \vec{g}|_{\rm rb}^{\rm T} \hat{P}_k|_{\rm rb}, \quad (10)$$

where ϕ_k is the angle between $\vec{g}|_{\rm rb}$ and $\hat{P}_k|_{\rm rb}$. Therefore, the voltage reading of the k^{th} accelerometer is given by

$$V_k = S_k \vec{g}|_{\rm rb}^{\rm T} \hat{P}_k|_{\rm rb} + \delta_k, \quad (11)$$

where $\hat{P}_k|_{\rm rb}$ and $\hat{P}_k|_{\rm ee}$ are defined in (8) and (6), respectively.

III. ROBOT KINEMATIC MANEUVER

To obtain data for calibration, we rotate the accelerometer in roll, pitch, and yaw and collect voltage readings. As a result of (10) and (11), the voltage reading of each accelerometer is proportional to the cosine of the angle between the accelerometer's orientation vector and the gravitational vector. Since the magnitude of the cosine function's derivative is greatest when ϕ_k is close to 90 deg, the voltage readings are most responsive to changes in sensor orientation when ϕ_k is close to 90 deg. Hence in this range, the voltage readings are most useful for data analysis. Therefore, it is necessary to rotate the arm so that ϕ_k is close to 90 deg for each accelerometer. However, the orientation vector of each accelerometer is unknown with respect to the end effector frame. We thus devise a maneuver that allows each accelerometer to provide a large number of voltage readings where $\cos\phi_k$ is close to 0 deg.

In our experiment, Link 1 of the robot arm is rotated θ_1 degrees about the $\hat{k}_{\rm rb}$-axis, performing yaw. As Link 1 is rotated, Link 5 of the robot arm is rotated θ_5 degrees in pitch while Link 6 is rotated θ_6 degrees, performing roll. The average angular velocities for links 1, 5, and 6 are 3.1 deg/s, 0.87 deg/s, and 13.9 deg/s, respectively. The entire maneuver takes 27.74 minutes to complete. Fig. **??** shows a graphical representation of this movement.

Data is collected at 166,400 link orientations at a sampling rate of 100 Hz. When analyzing the data, every 25th data point is taken so that the sampling rate is effectively 4 Hz. Since each subsequent orientation of the robot arm is close to that of the previous one, we assume that the robot arm is static, which allows us to ignore translational acceleration and angular velocity.

Each accelerometer has a range of ± 2 g with an output reading of between 0 V and 5 V. In addition, accelerometers

1, 2, and 3 have RMS noise levels of approximately 13.4 mV, 13.6 mV, 14.6 mV, respectively. These noise values were found by locking the arm in an orientation for 200 seconds at a sampling rate of 1 kHz. Performing this procedure for three different orientations of the robot arm, the RMS noise was then calculated for each of the three orientations, and the mean of these three values was taken as an approximation of the RMS noise level. From these values, accelerometers 1, 2, and 3 are found to have dynamic ranges of 51.4 dB, 51.3 dB, and 50.7 dB, which are equivalent to 8.54 bits, 8.52 bits, and 8.42 bits, respectively[3].

IV. Optimization Problems

To calibrate the triaxial accelerometer from the collected data, we formulate a least squares optimization problem using (11). Function minimization is performed using the $fminunc$ program in Matlab, which employs quasi-Newton minimization with numerical gradients. The $fminunc$ program thus utilizes the voltage readings from the accelerometers, the angular orientations of the robot links, the function to be optimized, and an initial estimate of the parameters. The initial estimates of the parameters are chosen so that each accelerometer's orientation vector is in the $+\hat{\imath}_{\rm ee}$ direction, each sensitivity is 1 V, and each bias is 2.5 V.

Two optimization problems are formulated. First, a calibration function is defined and optimized for each accelerometer, and, next, one calibration function is defined and optimized for all three accelerometers concurrently. We first calibrate the accelerometers separately to determine whether any of the sensors are faulty or whether the model is appropriate. Specifically, if the direction of gravity estimates obtained from the separate calibration vary by more than a few degrees, then the sensor, data, or model may need to be reexamined. Likewise, if each direction-of-gravity estimate in the separate calibration is within a few degrees, but the error in our estimates is large, we must examine our data and model for the cause of the large error. Define the data fit error ε_k of the parameter estimates for the k^{th} accelerometer to be

$$\varepsilon_k \triangleq \sqrt{\frac{\text{minimum value of } J_k}{\text{number of data points}}}. \tag{12}$$

A. Separate Accelerometer Calibration

First, we calibrate each accelerometer separately, assuming that the direction of gravity in the robot base frame is unknown. Therefore, the estimates of the direction of gravity can be different for each accelerometer. The magnitude of gravity g is assumed to be 9.8 $\mathrm{m/s^2}$. Let ϕ and ψ denote angular rotations about the $\hat{\jmath}_{\rm rb}$-axis and $\hat{k}_{\rm rb}$-axis of the robot base frame, respectively. Therefore, the direction of gravity $\hat{g}_k$ relative to the k^{th} accelerometer resolved in the robot base frame is

$$\hat{g}_k|_{\rm rb} = R_{\hat{k}}(\psi_k) R_{\hat{\jmath}}(\phi_k) \hat{\imath}_{\rm rb}, \tag{13}$$

where $R_{\hat{\jmath}}(\phi_k)$ and $R_{\hat{k}}(\psi_k)$ are the respective Euler rotation matrices about the $\hat{\jmath}_{\rm rb}$-axis and $\hat{k}_{\rm rb}$-axis for the k^{th} accelerometer. The voltage reading V_k for the k^{th} accelerometer is given by

$$V_k = 9.8 S_k \hat{g}_k|_{\rm rb}^{\rm T} \hat{P}_k|_{\rm rb} + \delta_k, \tag{14}$$

and the function to be optimized for the k^{th} accelerometer with 6 unknown parameters is

$$J_k(S_k, \hat{g}_k|_{\rm rb}, \hat{P}_k|_{\rm rb}, \delta_k) \triangleq \sum_{j=1}^{n} [V_{k,j} - (9.8 S_k \hat{g}_k|_{\rm rb}^{\rm T} \hat{P}_k|_{\rm rb} + \delta_k)]^2. \tag{15}$$

Here $V_{k,j}$ is the j^{th} voltage reading from the k^{th} accelerometer for a set of angles (θ_1,θ_5, θ_6) that determine the orientation of the end effector with respect to the robot base frame, taken n times, and $\hat{P}_k|_{\rm rb}$ is defined by (6) and (8).

B. Joint Accelerometer Calibration

After calibrating the accelerometers separately and examining the results, we calibrate the three accelerometers jointly. Therefore, the estimate of the direction of gravity is the same for each accelerometer; that is, there is only one unknown unit gravity vector in the optimization instead of three as in the separate calibration case. The accelerometer measurement model is the same as in (14), and the function to be minimized with respect to 14 unknown parameters is

$$J(S_1, S_2, S_3, \hat{g}|_{\rm rb}, \hat{P}_1|_{\rm rb}, \hat{P}_2|_{\rm rb}, \hat{P}_3|_{\rm rb}, \delta_1, \delta_2, \delta_3) \triangleq \sum_{k=1}^{3} J_k. \tag{16}$$

V. Optimization with Simulated Data

To assess the effectiveness of the optimization approach for obtaining parameter estimates, we calibrate the sensors using simulated data. We specify the sensitivity, bias, and orientation of each accelerometer, as well as the direction of gravity. We use these specified parameters to generate simulated voltage readings at 6656 link orientations. In addition, we add white noise to the simulated measurements. The resulting parameter estimates are compared to the actual parameter values to assess their accuracy.

A. Separate Accelerometer Calibration

First, we consider the precision of the optimization involving the function (15). For convenience, let gravity point in the $-\hat{k}_{\rm rb}$ direction, although this direction is unknown to the optimization procedure. Assume there is no noise in the measurements. The parameters used to generate the simulated data are given in Table II. When there is no noise, the optimization yields highly accurate parameter estimates.

Next, white noise is added to the simulated data. For comparison purposes, the optimization is performed with noise that is distributed normally on an interval centered about zero chosen to have a standard deviation equal in size to the RMS noise level of the respective accelerometer and then with the standard deviation increased by a factor of 10. The notation $N(a, b)$ is used to denote the normal distribution with mean a and standard deviation b. For accelerometer 1, the two noise distributions used are $N(0, 0.0134)$ and $N(0, 0.134)$.

TABLE II

PARAMETER VALUES USED TO GENERATE THE SIMULATED DATA. THE NUMERICAL SIMULATION IS USED TO ASSESS POSSIBLE INCONSISTENCY IN THE PRESENCE OF NOISE.

accelerometer	β_k (deg)	γ_k (deg)	S_k (Vs^2/m)	δ_k (V)
1	-89	2	0.1	2.45
2	1	93.5	0.15	2.55
3	-3.75	-2	0.095	2.3

Optimization with noisy simulated data is performed for an increasing number of data points. If the parameter estimates converge to the actual parameter values as the number of data points used in the optimization increases, then the estimator may be consistent [4].

The estimates of S_1 and δ_1 nearly converge to the actual estimates when the noise has a distribution of $N(0, 0.0134)$. For the sensitivity of accelerometer 1, the estimate is close to the actual value at about 1000 data points. In addition, the offset estimate of accelerometer 1 appears to be converging to the actual parameter value. From about 2500 data points onward, the estimate for the offset stays within 0.0001 V of the actual value. Therefore, when we calibrate the accelerometers using this procedure, the estimator might be slightly inconsistent. For the case in which the noise has a distribution of $N(0, 0.134)$, the estimates appear to be converging.

B. Joint Accelerometer Calibration

For the function defined in (16), we examine the consistency of the parameter estimates in the same manner. The actual parameters are those given in Table II, and the measurement noise is the same as for the separate accelerometer calibration. When there is no noise, the optimization provides accurate estimates with small errors, as it did for separate calibration. In addition, when white noise is added to the simulated data, the estimates appear to converge to the actual parameter values.

When the noise of accelerometer 1 has a distribution of $N(0, 0.0134)$, the sensitivity estimates reach the actual parameter value at about 1000 data points. The offset estimate is within 0.0003 V of the actual parameter value at about 6500 data points. These results suggest that this estimate may be slightly inconsistent. If the noise distribution has a greater standard deviation, then the accuracy of the estimates degrades.

VI. OPTIMIZATION WITH EXPERIMENTAL DATA

We now calibrate each accelerometer with experimental data. Using the data generated by the kinematic maneuver, we optimize the functions given in Section 4 to estimate the sensitivity, bias, and unit orientation vector of each accelerometer, as well as the direction of gravity.

A. Separate Accelerometer Calibration

Optimizing (15) for each accelerometer yields the results shown in Table III. The data fit errors in the parameter

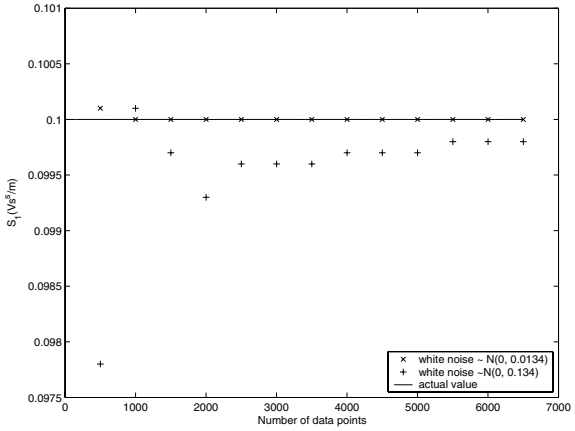

Fig. 1. Parameter estimates S_1 for accelerometer 1 with an increasing number of simulated data points using joint accelerometer calibration.

TABLE III

OPTIMIZATION RESULTS FOR SEPARATE ACCELEROMETER CALIBRATION. ψ_k ABOUT THE $\hat{z}_{\mathrm{rb}}$-AXIS DO NOT CHANGE THE

accelerometer	β_k (deg)	γ_k (deg)	S_k (Vs^2/m)	δ_k (V)
1	85.3089	89.8536	0.14259	2.3757
2	-1.2396	0.89466	0.14251	2.4491
3	1.2837	272.1405	0.14197	2.1096

accelerometer	ϕ_k (deg)	ψ_k (deg)
1	89.7507	351.3317
2	89.9933	94.3114
3	89.8723	216.0829

accelerometers	angle between (deg)
1 and 2	91.1503
1 and 3	93.4037
2 and 3	88.7825

estimates for accelerometers 1, 2, and 3 are 18 mV, 26 mV, and 26 mV, respectively. Note that the estimates of the angles ϕ_k and ψ_k that determine the direction of gravity vary slightly. However, since ϕ_k varies by less than 0.25 deg $\hat{g}_k|_{\mathrm{rb}}$ is close to the same direction for each accelerometer. Therefore, it appears that our model may not have a fundamental problem discernable from separate estimation of $\hat{g}_k|_{\mathrm{rb}}$, and we now calibrate the accelerometers jointly.

B. Joint Accelerometer Calibration

Minimizing the function (16) yields the results displayed in Table IV. The data fit error in the parameter estimates for accelerometers 1, 2, and 3 is 41 mV. This error is less than the sum of the errors in the separate calibration case, suggesting that the joint calibration parameter estimates may be more accurate.

To analyze the dependence of the parameter estimates in Table IV on the chosen data subset, we perform the same optimization 25 times. Specifically, we take each 25th data point of the entire set of 166,400 data points, perform the optimization, and then repeat with an offset data set. The

TABLE IV

OPTIMIZATION RESULTS FOR JOINT ACCELEROMETER CALIBRATION.

accelerometer	β_k (deg)	γ_k (deg)	S_k (Vs^2/m)	δ_k (V)
1	85.3089	89.8537	0.14259	2.3754
2	-1.2394	0.8943	0.14251	2.4491
3	1.2829	272.1489	0.14198	2.1096

accelerometer	ϕ (deg)	ψ (deg)
1, 2, 3	90.0023	11.0511

accelerometers	angle between (deg)
1 and 2	91.1501
1 and 3	93.4044
2 and 3	88.7738

TABLE V

ANALYSIS OF THE JOINT ACCELEROMETER CALIBRATION USING 25 DATA SETS.

accelerometers	parameter	mean	std. dev.
1	S_1 (Vs^2/m)	0.1426	2.8356×10^{-5}
1	δ_1 (V)	2.3755	1.8572×10^{-4}
1	β_1 (deg)	85.3442	0.0170
1	γ_1 (deg)	89.8377	0.1579
2	S_2 (Vs^2/m)	0.1425	4.1989×10^{-5}
2	δ_2 (V)	2.4492	2.6657×10^{-4}
2	β_2 (deg)	-1.2566	0.0230
2	γ_2 (deg)	0.8681	0.0265
3	S_3 (Vs^2/m)	0.1421	5.0368×10^{-5}
3	δ_3 (V)	2.1093	2.8925×10^{-4}
3	β_3 (deg)	1.3023	0.0199
3	γ_3 (deg)	272.1241	0.0320
gravity	ϕ (deg)	90.0159	0.0288
gravity	ψ (deg)	134.1036	88.7530

mean and standard deviation of the 25 estimates of each parameter are shown in Table V. The parameter estimates in Table IV are all within 1 standard deviation of the corresponding mean parameter estimate, indicating that the estimates are independent of the data subset.

VII. MAGNETOMETER

In addition to calibrating the triaxial accelerometer, we calibrate the triaxial magnetometer packaged in the 3DM Sensor. The magnetometer measures the Earth's magnetic field, displaying these readings from 0 V to 5 V. The RMS noise levels of magnetometers 1, 2, and 3 are 8.5 mV, 6.8 mV, and 11.7 mV, respectively, found in the same manner as for the accelerometers. The dynamic ranges of magnetometer 1, 2, and 3 are 55.4 dB, 57.3 dB, and 52.6 dB, which are equivalent to 9.20 bits, 9.52 bits, and 8.74 bits, respectively.

Define a vector $\vec{B}$ representing the Earth's magnetic field as felt by each magnetometer, in the robot base frame, to be

$$\vec{B}|_{\mathrm{rb}} = \begin{bmatrix} B_{\mathrm{x}} \\ B_{\mathrm{y}} \\ B_{\mathrm{z}} \end{bmatrix}. \tag{17}$$

The magnitude of the Earth's magnetic field felt by the magnetometers is assumed for convenience to be 1 G, where G denotes Gauss. The voltage reading V_k of the k^{th} magnetometer is

$$V_k = S_k B_k + \delta_k, \tag{18}$$

where S_k, δ_k, and B_k are the sensitivity of the k^{th} magnetometer, the offset of the k^{th} magnetometer, and the Earth's magnetic field at the axis of the k^{th} magnetometer, respectively. Let the unit orientation $\hat{P}|_{\mathrm{rb}}$ of each magnetometer resolved in the robot base frame be defined by (6) and (8), and let ϕ_k be the angle between $\vec{B}|_{\mathrm{rb}}$ and $\hat{P}_k|_{\mathrm{rb}}$. Therefore, the component of the Earth's magnetic field felt by the k^{th} magnetometer is

$$\vec{B}_k = \vec{B}|_{\mathrm{rb}}^{\mathrm{T}} \hat{P}_k|_{\mathrm{rb}} = |\vec{B}||\hat{P}_k| \cos\phi_k, \tag{19}$$

and the voltage reading V_k for the k^{th} magnetometer is

$$V_k = S_k \vec{B}|_{\mathrm{rb}}^{\mathrm{T}} \hat{P}_k|_{\mathrm{rb}} + \delta_k. \tag{20}$$

A. Magnetometer Calibration

To estimate the unknown magnetometer parameters S_k, δ_k, $\vec{B}_k|_{\mathrm{rb}}$, and $\hat{P}_k|_{\mathrm{rb}}$, we perform two different calibrations, as for the accelerometers. Again, this approach provides a check of the fundamental structure of the model and integrity of the data. The kinematic maneuver described in Section 3 is used to generate the experimental data used in the optimizations.

First, we define a function to separately calibrate the magnetometers. Therefore, the Earth's magnetic field located at the magnetometer's axis is estimated in each function optimization. The function to be minimized for the k^{th} magnetometer with 6 unknown parameters is

$$J_k(S_k, \hat{B}_k|_{\mathrm{rb}}, \hat{P}_k|_{\mathrm{rb}}, \delta_k) \triangleq \sum_{j=1}^{n} [V_{k,j} - (S_k \hat{B}_k|_{\mathrm{rb}}^{\mathrm{T}} \hat{P}_k|_{\mathrm{rb}} + \delta_k)]^2. \tag{21}$$

Optimization of (21) results in the parameter estimates displayed in Table VI. The data fit errors in the parameter estimates of magnetometers 1, 2, and 3 are 0.1179 V, 0.150 V, and 0.1257 V, respectively. These error values are all approximately 0.1 V greater than the corresponding errors for the separately calibrated accelerometers, suggesting that the

TABLE VI

PARAMETER ESTIMATES FOUND USING SEPARATE MAGNETOMETER CALIBRATION.

magnetometer	β_k (deg)	γ_k (deg)	S_k (V/G)	δ_k (V)
1	0.96609	270.1986	1.3014	2.4216
2	-85.628	185.9308	1.329	2.3965
3	-4.0163	1.216	1.3342	2.7643

magnetometer	ϕ_k (deg)	ψ_k (deg)
1	59.5327	81.4606
2	59.2785	80.7460
3	59.4192	81.3364

magnetometers	angle between (deg)
1 and 2	90.5314
1 and 3	91.0743
2 and 3	90.3379

TABLE VII

PARAMETER ESTIMATES USING JOINT MAGNETOMETER CALIBRATION.

magnetometers	β_k (deg)	γ_k (deg)	S_k (V/G)	δ_k (V)
1	0.96237	270.2059	1.3006	2.4216
2	-85.6307	185.8359	1.3283	2.3967
3	-4.0172	1.2153	1.3342	2.7643

magnetometers	ϕ_k (deg)	ψ_k (deg)
1, 2, 3	59.4127	81.402

magnetometers	angle between (deg)
1 and 2	90.5314
1 and 3	91.0742
2 and 3	90.3379

parameter estimates for the magnetometers may not be as accurate as the parameter estimates for the accelerometers. One cause of the greater data fit error could be due to stray magnetic fields from which we could not isolate the sensor. The estimates of ϕ_k and ψ_k are within 0.26 deg and 0.72 deg, respectively.

Next, we calibrate the magnetometers jointly. One function is formulated and optimized for all 3 magnetometers, and one Earth's magnetic field vector is estimated. Similar to the case of joint accelerometer calibration, the resulting cost function with 14 unknown parameters is

$$J(S_1,S_2,S_3,\hat{B}|_{\rm rb},\hat{P}_1|_{\rm rb},\hat{P}_2|_{\rm rb},\hat{P}_3|_{\rm rb},\delta_1,\delta_2,\delta_3)\triangleq\sum_{k=1}^{3} J_k(S_k,\hat{B}_k|_{\rm rb},\hat{P}_k|_{\rm rb},\delta_k) \tag{22}$$

Minimizing (22) produces the parameter estimates displayed in Table VII. The error in the parameter estimates is 0.2285 V. This error is less than the sum of the errors in the separate magnetometer calibrations. This finding suggests that calibrating the magnetometers jointly produces more accurate parameter estimates with a smaller error than calibrating the magnetometers separately.

To analyze the dependence of the parameter estimates resulting from the optimization of (22) on the data subset, we perform the optimization 25 times using the same procedure as for the accelerometers. The mean and standard deviation of the parameter estimates are displayed in Table VIII. The parameter estimates in Table VII are all within 1 standard deviation of the corresponding mean estimates in Table VIII. This closeness suggests that the estimates are independent of the data subset.

VIII. CONCLUSIONS

In this paper, we derived a kinematic model and kinematic maneuver to calibrate a triaxial accelerometer and magnetometer. The calibration was accomplished by implementing this maneuver on a six-degree-of-freedom robotic arm. Analysis of the accuracy of our experimental results was performed by generating simulated data, formulating two optimization problems, and computing the data fit error of the parameter estimates. By first calibrating the accelerometers with simulated data, we evaluated the possibility of inconsistency in our estimator. By calibrating the accelerometer and magnetometer separately, we were able to check for discrepancies in the data and model. The joint calibrations produced smaller errors for both the magnetometer and accelerometer than did the separate calibrations, implying that the results from the joint calibrations may be more accurate. In addition, we tested the dependence of the parameter estimates on the data subset by repeating the joint calibrations of the accelerometer and magnetometer 25 times with different data sets and, then, computing the mean and standard deviation of the 25 estimates. The results from this analysis suggest that varying the data set may not change our estimate by a relatively large amount, suggesting that the parameter estimates for the joint calibration are independent of the chosen data subset the collected data.

TABLE VIII

ANALYSIS OF THE JOINT CALIBRATION FOR THE MAGNETOMETERS USING 25 DATA SETS.

magnetometers	parameter	mean	std. dev.
1	S_1 (V/G)	1.3013	2.7656×10^{-4}
1	δ_1 (V)	2.4217	1.2231×10^{-4}
1	β_1 (deg)	0.9672	0.0091
1	γ_1 (deg)	270.2025	0.0074
2	S_2 (V/G)	1.3285	1.8814×10^{-4}
2	δ_2 (V)	2.3967	1.3098×10^{-4}
2	β_2 (deg)	-85.6327	0.0082
2	γ_2 (deg)	185.9310	0.1691
3	S_3 (V/G)	1.3344	2.3063×10^{-4}
3	δ_3 (V)	2.7643	1.0935×10^{-4}
3	β_3 (V)	-4.0152	0.0073
3	γ_3 (V)	1.2193	0.0113
Magnetic Field	ϕ (deg)	59.4153	5.4911×10^{-5}
Magnetic Field	ψ(deg)	81.2401	2.0431×10^{-4}

IX. ACKNOWLEDGMENTS

The authors gratefully acknowledge the contribution of Jacob Apkarian of Quanser, Inc. and Steve Arms and Dave Churchill of Microstrain, Inc.

REFERENCES

[1] J. Hall, R. Williams II, and F. Grass, "Inertial Measurement Unit Calibration Platform," in *Proceedings of the Sixth Conference on Applied Mechanisms and Robotics*, Cincinnati, OH, Dec. 1999.

[2] L. Sciavicco and B. Siciliano, *Modelling and Control of Robot Manipulators*, 2nd ed., London: Springer, 2002.

[3] D. S. Bernstein, "Sensor Performance Specifications," *IEEE Control Systems Mag*, pp. 9-18, Aug. 2001.

[4] J.E. Freund, I. Miller, and M. Miller, *Mathematical Statistics*, 6th ed., Upper Saddle River, NJ: Prentice Hall, 1999.